Advantages and Tuning of Zero Voltage Switching in a Wireless Power Transfer System

Grazian, Francesca; Van Duijsen, Peter; Soeiro, Thiago B.; Bauer, Pavol

DOI
10.1109/WoW45936.2019.9030626

Publication date
2019

Published in
2019 IEEE PELS Workshop on Emerging Technologies

Advantages and Tuning of Zero Voltage Switching in a Wireless Power Transfer System

Francesca Grazian, Peter van Duijsen, Thiago B. Soeiro, Pavol Bauer
Delft University of Technology
The Netherlands
Email: (F.Grazian, P.J.vanDuijsen, T.BatistaSoeiro, P.Bauer)@tudelft.nl

***Abstract*—In charging applications, wireless power transfer (WPT) is mostly used in the form of inductive power transfer with magnetic resonant coupling. Therefore, both the transmitter and the receiver coils are combined with capacitors, such that only active power is transferred. To evaluate the operation of the WPT charging system, its equivalent circuit can be analyzed in the frequency domain. However, this is limiting since the H-bridge inverter operation is not intrinsically considered. As an example, the operating points of both zero current switching (ZCS) and zero voltage switching (ZVS) operations might be still analyzed, but it is not possible to assess their performance in terms of efficiency. In this paper, the advantage of ZVS over the ZCS is evaluated in terms of the efficiency and the delivered output power. To enable the full potential of ZVS, this is tuned considering the switch capacitance and the dead time.**

***Index Terms*—Efficiency, Inverter control, wireless power transfer (WPT), zero voltage switching (ZVS), zero current switching (ZCS)**

I. Introduction

According to [1], radio-frequency wireless technologies can be divided into three categories: wireless communication of data, wireless sensing and wireless power transfer (WPT). In WPT, a considerable amount of energy is sent from the transmitter to the receiver and the two most common applications are energy harvesting (solar) and battery charging. In wireless charging, inductive power transfer with magnetic resonant coupling is generally used [2]–[4], in which the transmitter and receiver are loosely coupled coils. The inductive power of these coils is compensated by capacitors, such that only active power is transferred. These capacitors with the coils form resonant circuits and, depending on the configuration, the compensation network can be either series-series (S-S), series-parallel (S-P), parallel-series (P-S) or parallel-parallel (P-P) [5]–[7], as shown in Fig. 1. Any of these compensation networks can be analyzed in the frequency domain through their relative phasor equations, which can be computed from the equivalent circuits shown in Fig. 1. This analysis relies on the fundamental harmonic approximation (FHA) named in [8], which considers all voltages and currents to be sinusoids operating at the chosen frequency. The FHA describes well the behavior of the resonant circuits and different operating points can be analyzed in the frequency domain. Using this approach, it is possible to have a first estimation of the voltage and current values in both circuits at different operating frequencies. As an example, the operation at zero current switching (ZCS) can be analyzed by imposing the power factor (PF) of the primary circuit to be unity. This means that the ZCS occurs at the frequency that gives a zero phase shift between the primary voltage and current. The zero voltage switching (ZVS) operation can also be analyzed through the equivalent circuit imposing circulating reactive power by making the primary current lagging the fundamental frequency component of the primary voltage. However, evaluating the performance of ZCS and ZVS in terms of efficiency is not possible only by using the equivalent circuits in Fig. 1, because the inverter is not included in this analysis. In reality, the inverter supplies the source (either voltage or current) at a chosen operating frequency and its losses have impact on the total efficiency. Moreover, the inverter's output is a square wave instead of a sinusoid, that makes the FHA more critical as the PF differs from unity.

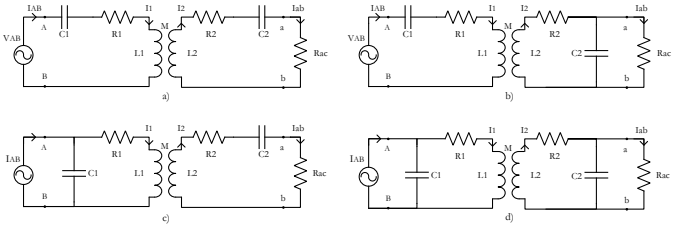

Fig. 1: Compensation networks: a) S-S, b) S-P, c) P-S, d) P-P.

This paper analyzes the advantages of ZVS over the ZCS operation in a S-S compensation network. Among all the possible compensation networks, S-S is taken into account because it is the only one in which the compensation capacitance values are independent of both the coupling and the load [5], [6], [9]. The minimum ZVS operating point is tuned considering the dead time and the switch capacitance. Then, the optimum operating point for ZVS is defined in terms of efficiency and amount of power delivered to the output. Measurements on an e-bike WPT charging system are executed as a proof of concept. The equivalent circuit of the used WPT charging system is shown in Fig. 2, which consists of an H-bridge inverter, a S-S compensation network, a diode-bridge rectifier and a resistive load.

The analysis in the frequency domain based on the FHA is explained in Section II. Then, the characteristics of both the ZCS and the ZVS operations are discussed in Section III.

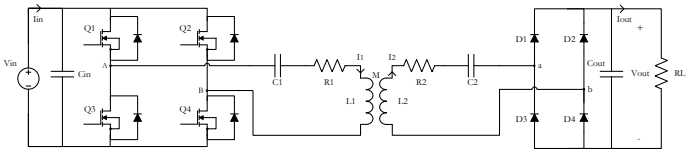

Fig. 2: WPT charging system.

In Section IV, the minimum operating point that gives ZVS is tuned at different input voltage and dead time conditions. The measured performance of ZVS in terms of efficiency and output power is compared to ZVC in Section V. The results of this analysis are discussed in Section VI. Finally, Section VII gives some conclusions on the ZVS tuning.

II. FHA ANALYSIS

From the equivalent circuit in Fig. 1 a), the equations for the primary and secondary circuit can be computed as in (1) and (2) using the Kirchhoff's voltage law. The mutual inductance M is computed through the coupling factor k and the coil inductances L_1 and L_2 as in (3). According to [10]–[12], it is possible to define an equivalent load resistance R_{ac} as in (4) for the analysis in the frequency domain, where R_L is the equivalent resistive load after the rectifier stage in Fig. 2. In turn, R_L models the charging behavior of the battery at a specific operating point of voltage and current.

$$\boldsymbol{V}_{AB} = (R_1 + j\omega L_1 + \frac{1}{j\omega C_1})\boldsymbol{I}_1 + j\omega M \boldsymbol{I}_2 \tag{1}$$

$$0 = j\omega M \boldsymbol{I}_1 + (R_2 + R_{ac} + j\omega L_2 + \frac{1}{j\omega C_2})\boldsymbol{I}_2 \tag{2}$$

$$M = k\sqrt{L_1 L_2} \tag{3}$$

$$R_{ac} = \frac{8}{\pi^2} R_L \tag{4}$$

The FHA analysis using (1)−(4) can be used as frequency analysis of the equivalent circuit's operating points. However, the performance of these operating points in terms of both efficiency and delivered output power cannot be evaluated only by using the FHA model, because the influence of the inverter is not included. Therefore, their performance must be assessed by considering the whole WPT charging system in Fig. 2.

III. ZCS AND ZVS

ZCS occurs when there is no current flowing through the switch during the switching transition. In the WPT charging system of Fig. 2, it is possible to achieve the ZCS at both turn-on and turn-off by detecting the zero-crossing of i_1 and switching the inverter leg exactly at that moment. The fundamental component of v_{AB} and i_1 are in phase which means that the PF is unity. Therefore, i_1 does not have large harmonic components which is good for electromagnetic compatibility (EMC). On the other hand, the drain-source capacitance C_{ds} of the switch is not completely discharged and, at turn-on, its charge is dissipated inside the switch. In case of short dead time t_{dead}, it might be difficult to tune the switching exactly at the zero-crossing of i_1 and the ZCS could be lost.

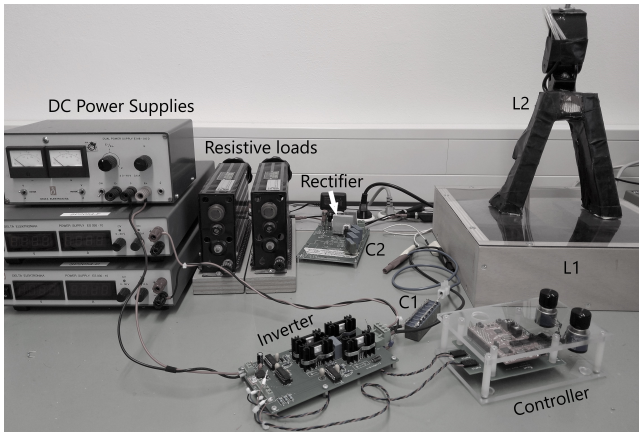

Fig. 3: Picture of the laboratory set-up: e-bike WPT charging system.

ZVS occurs when the voltage across the switch is zero during the switching transition. As explained in [11], it is generally easier to achieve this condition at the turn-off, because during the conduction the voltage across the switch is 1-2 V and, in case of MOSFETs, the current drops to zero fast enough. On the other hand, at turn-on, the switch voltage goes from the blocking voltage V_{in} (considering an H-bridge) to its conduction value. The ZVS is realized if the switch starts conducting when the voltage across the switch is already equal to the conduction value. According to [7], it is possible to realize this in the WPT charging system of Fig. 2, by making sure that i_1 lags v_{AB}. Therefore, considering the half period in which Q_2 and Q_3 are conducting and i_1 is negative, these two switches must be turned off while the current is still negative and the anti-parallel diodes of Q_1 and Q_4 would start conducting. After this, Q_1 and Q_4 must be turned on when i_1 is still negative such that they would naturally take i_1 from the diodes when it becomes positive. The reverse recovery would also not occur [13] and ZVS is achieved. In [14] and [15], the minimum amount of negative current I_{OFF} that assures the ZVS is defined as in (5). The ZVS operation does not have a completely unity PF, but the overall losses could be reduced especially in case of large C_{ds}.

$$I_{OFF} > \frac{2C_{ds}V_{in,max}}{t_{dead}} \tag{5}$$

The value of I_{OFF} should be kept low such that the turn-off is also a soft-switching. However, in case of an under-estimation of I_{OFF}, ZVS at turn-off can be lost.

IV. TUNING OF I_{OFF}

According to (5), it is clear that the value of the negative current I_{OFF} can be tuned by setting an appropriate t_{dead}. The value of C_{ds} also plays a role in this tuning. In MOSFETs, C_{ds} is highly dependent on the blocking drain-source voltage V_{ds} which is equal to V_{in} in a H-bridge inverter. The dependence of C_{ds} on V_{in} is an intrinsic property of each MOSFET and it depends on the packaging and manufacturing

TABLE I: Parameters in the laboratory set-up.

k	L_1(µH)	L_2(µH)	C_1(nF)	C_2(nF)	$R_1(\Omega)$	$R_2(\Omega)$
0.28	67.7	46.3	35.9	52.3	0.11	0.16

conditions of a certain device. In this analysis, the device used is IPP030N10N5 which is a 100V MOSFET with a nominal conduction resistance $R_{ds(on)}$ lower than $3\,\mathrm{m}\Omega$. From the device's datasheet [16], the output and the reverse transfer capacitances C_{oss} and C_{rss} are known depending on V_{ds}. Therefore, C_{ds} can be computed as $C_{ds} = C_{oss} - C_{rss}$. Typical values of C_{ds} are shown in Table II. Other parasitic capacitances from the resonant circuits may add to C_{ds}, but for this WPT charging system they have been found negligible.

In this paper, the analyzed WPT charging system is used to charge e-bikes. Therefore, the target load is typically a low-voltage battery which ranges between 24-48 V. A picture of the laboratory set-up used as a proof of concept is shown in Fig. 3, in which the secondary coil is the double kickstand of the bike and the primary coil is placed under a charging tile which is placed on the ground. The circuit schematic is equal to the one in Fig. 2 and each component's value has been experimentally resumed and can be found in Table I.

To gain an initial understanding of the ZVS operation, the minimum I_{OFF} values at three conditions of V_{in} and t_{dead} have been computed according to (5) and they are shown in Table II. It is clear how the minimum I_{OFF} decreases when t_{dead} becomes larger. This happens because, at the same voltage condition, that capacitance has more time to discharge and, consequently, it requires less current. These theoretical values of I_{OFF} are compared with measurements on a laboratory set-up that have been done at the same V_{in} and t_{dead} conditions, using a resistive load $R_L = 10\,\Omega$. The measured values of I_{OFF} are shown in Fig. 4 together with the theoretical ones of Table II. According to the plot in Fig.4 and as expected, the measured I_{OFF} values are higher than their respective theoretical ones.

The output power and efficiency have also been measured at the same I_{OFF}, V_{in} and t_{dead} as shown in Fig. 4, and these are plotted in Fig. 5. The efficiency $\eta_{\%}$ is computed as defined in (6), referring to the DC input and DC output power of Fig. 2.

$$\eta_{\%} = \frac{V_{out} I_{out}}{V_{in} I_{in}} \cdot 100 = \frac{P_{out}}{P_{in}} \cdot 100 \tag{6}$$

V. Comparison between ZCS and ZVS

A. Performance at the minimum I_{OFF} value

After measuring the performance at ZVS, both the output power and the efficiency are compared respectively with the ones achieved at ZCS in Fig. 6 and 7 for the same V_{in} and t_{dead} conditions. In case of ZCS, the only two differences are that I_{OFF} is equal to zero and, obviously, that ZVS and ZCS work at different operating frequencies. It is possible to tune both the frequency and t_{dead} of the inverter with the two potentiometer knobs of the controller in Fig. 3.

TABLE II: Theoretical values of I_{OFF} from (5).

V_{in} (V)	C_{ds} (nF)	t_{dead} (ns)	I_{OFF}(A)
24	2.30	100	1.10
		200	0.55
		400	0.28
36	1.72	100	1.24
		200	0.62
		400	0.31
48	1.13	100	1.08
		200	0.54
		400	0.27

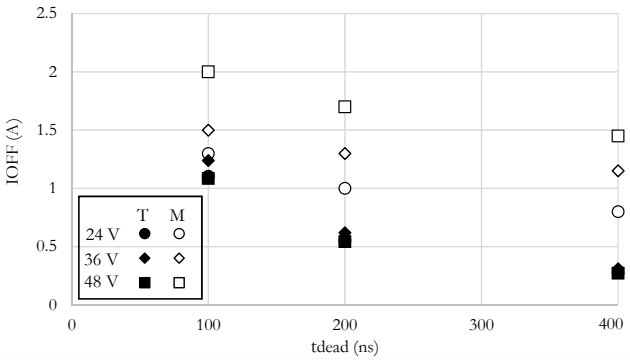

Fig. 4: I_{OFF} at V_{in} =24, 36, 48 V. T= theoretical, M= measured values.

B. Performance at higher I_{OFF} values

It is difficult to ensure that the operation is always at an exact point for any possible circuit condition. Therefore, to complete the tuning of the ZVS, it is important to analyze the performance of the WPT charging system when the values of I_{OFF} are higher than the minimum measured values in Fig. 4. For higher values of I_{OFF}, the operation would still be ZVS. However, if I_{OFF} becomes too high, the turn-off losses could become considerable and, at some point, they could have a negative impact on the overall efficiency. To evaluate the performance of these operating points, measurements have been executed at $V_{in} = 48\,\mathrm{V}$ and t_{dead} =100, 200, 400 ns and their measured output power and efficiency are plotted respectively in Fig. 8, 9 and 10. In all these charts, four values of I_{OFF} are shown in which the first value corresponds to ZCS ($I_{OFF} = 0\,\mathrm{A}$), the second value corresponds to the minimum value of I_{OFF} such that ZVS is achieved in that condition (according to Table II) and the other two are higher values that give ZVS. In all measurements, the case of ZVS with the minimum value of I_{OFF} gives the best performance with respect to both output power and efficiency.

VI. Discussion of the results

Based on the results shown in the previous sections, some considerations need to be pointed out.

- According to Fig. 4, the measured I_{OFF} minimum values that ensure ZVS become smaller as t_{dead} enlarges. This measured trend of I_{OFF} agrees with the theoretical trend from (5). However, the measured values are greater than the theoretical ones at all V_{in} and t_{dead} conditions. This result can be due to many factors. Firstly, the calculation of I_{OFF}

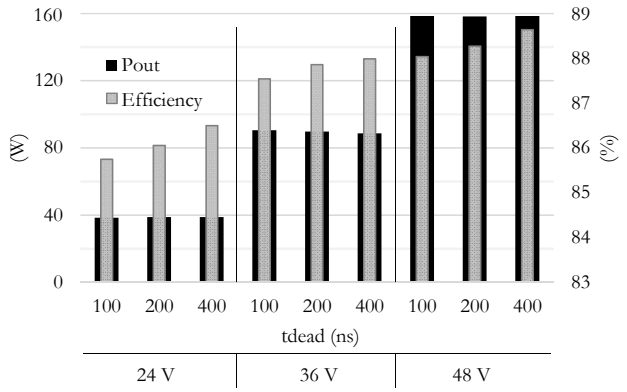

Fig. 5: Measured output power and efficiency achieved with ZVS, operating at the measured I_{OFF} values of Fig. 4.

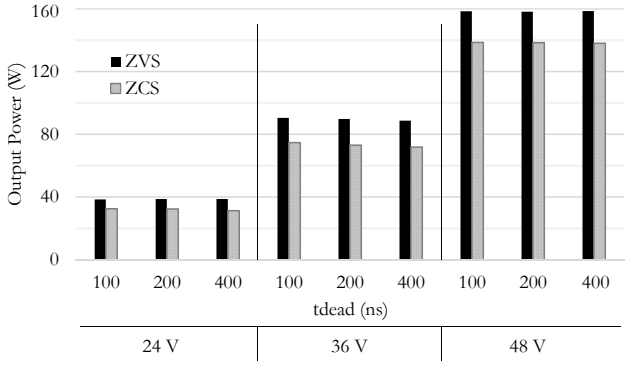

Fig. 6: Measured output power values at both ZVS and ZCS operations, at the same V_{in} and t_{dead} conditions as in Table II.

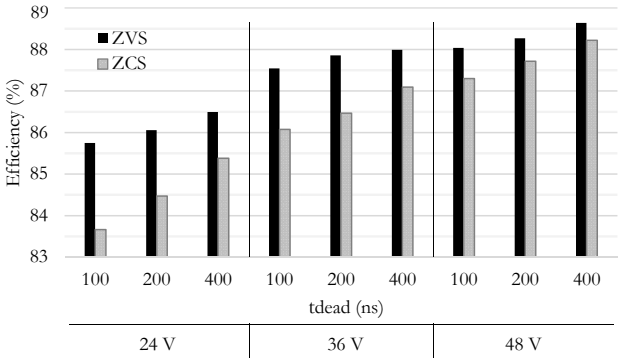

Fig. 7: Measured efficiency values at both ZVS and ZCS operations, at the same V_{in} and t_{dead} conditions as in Table II.

in (5) assumes that the current is constant during the whole t_{dead}. Nevertheless, the current is actually a high-frequency sinusoid which makes this assumption weak in a first place. Moreover, the values of the internal capacitances C_{oss} and C_{rss} specified in the MOSFET's datasheet are not measured at the same gate-source voltage and frequency conditions as the operation of the WPT charging system. This means that the actual value of C_{ds} could be different from the theoretical one. On top of that, there might be other parasitic capacitances that need to be discharged in that interval, so they could add to C_{ds}. Therefore, the definition of I_{OFF} in (5) must be used only to have an initial insight and a margin must be considered during the actual operation.

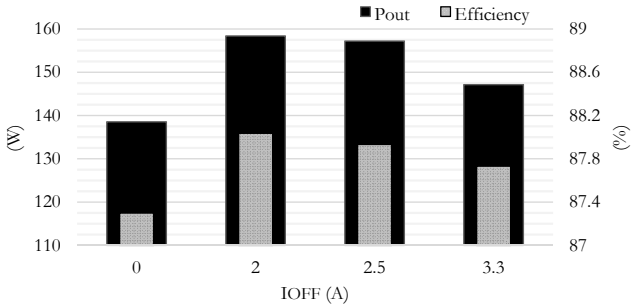

Fig. 8: Measured output power and efficiency with different I_{OFF}, at $V_{in} = 48\,\text{V}$, $R_L = 10\,\Omega$ and $t_{dead} = 100\,\text{ns}$.

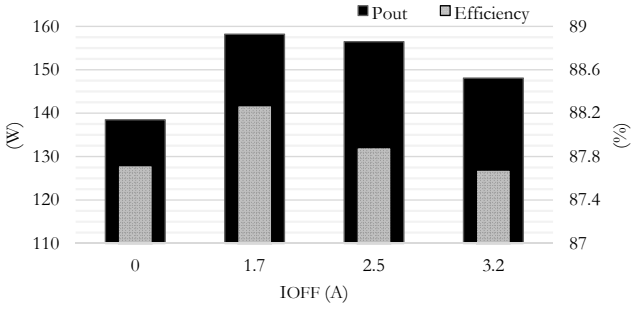

Fig. 9: Measured output power and efficiency with different I_{OFF}, at $V_{in} = 48\,\text{V}$, $R_L = 10\,\Omega$ and $t_{dead} = 200\,\text{ns}$.

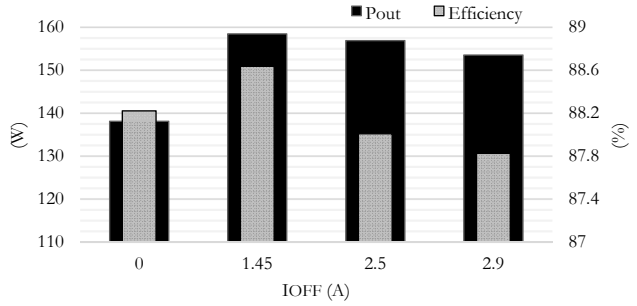

Fig. 10: Measured output power and efficiency with different I_{OFF}, at $V_{in} = 48\,\text{V}$, $R_L = 10\,\Omega$ and $t_{dead} = 400\,\text{ns}$.

- According to Fig. 5, it is clear that, for all the values of V_{in}, the reached efficiency is lower with for shorter t_{dead}. Two main reasons have been identified. Firstly, when t_{dead} is shorter, there is a small margin to realize the soft-switching. On the other hand, when t_{dead} is longer, it is easier to make sure that C_{ds} is completely discharged and, as a consequence, the efficiency is higher. These observations are also confirmed by Fig. 11 and 12 which shows the measured waveforms at both ZCS and ZVS respectively for $t_{dead} = 100\,\text{ns}, 200\,\text{ns}$. According to Fig. 11 b), for $t_{dead} = 100\,\text{ns}$ the ZVS is not perfectly reached because there is still some overshoot in V_{ds} turn-off. However, that overshoot is definitely lower than the one at ZCS operation shown in Fig. 11 a). On the other hand, Fig. 12 b) shows that with $t_{dead} = 200\,\text{ns}$ the overshoot of V_{ds} is not present. The second reason why the reached efficiency is lower when t_{dead} is short is that, as shown in Fig. 4, the minimum value of I_{OFF} is greater than in the case with larger t_{dead}. Therefore, the turn-off switching losses are also higher and

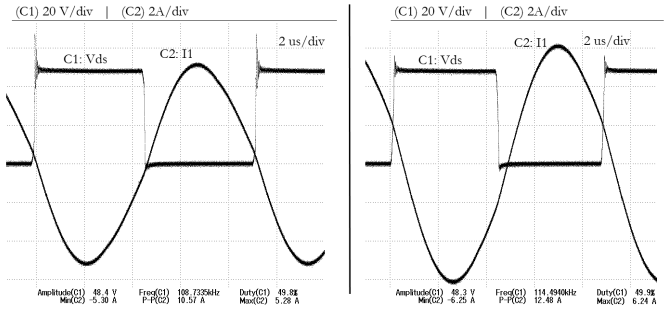

Fig. 11: Measured waveforms V_{ds} and i_1 at $V_{in} = 48\,\text{V}$ and $t_{dead} = 100\,\text{ns}$: a) ZCS, b) ZVS.

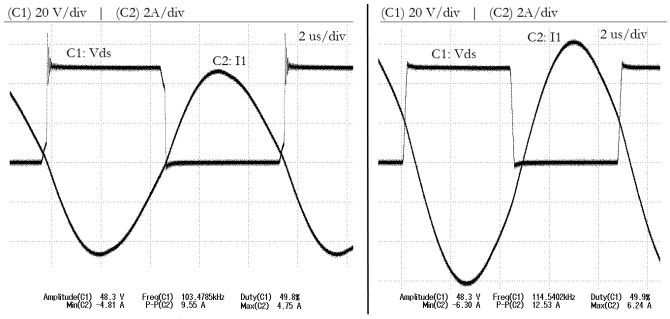

Fig. 12: Measured waveforms V_{ds} and i_1 at $V_{in} = 48\,\text{V}$ and $t_{dead} = 200\,\text{ns}$: a) ZCS, b) ZVS.

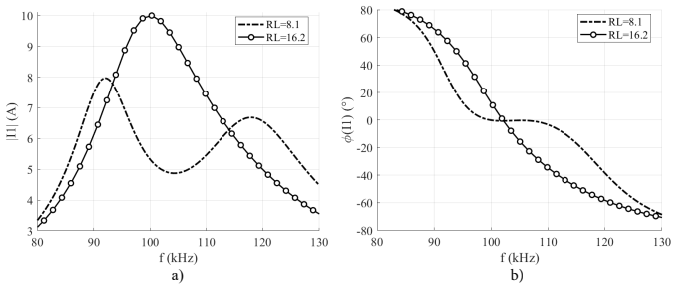

Fig. 13: Frequency analysis of $\boldsymbol{I}_1$ at $V_{in} = 48\,\text{V}$ through (1) and (2): a) absolute value $|\boldsymbol{I}_1|$, b) phase angle $\phi(\boldsymbol{I}_1)$.

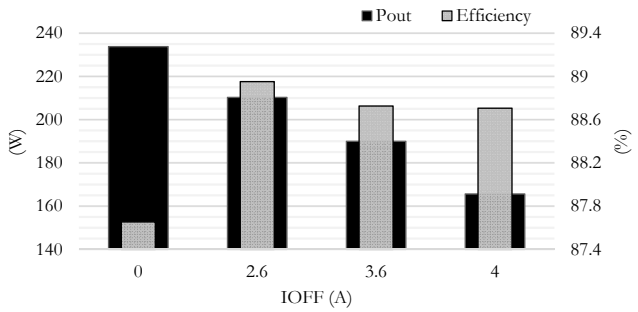

Fig. 14: Measured output power and efficiency with different I_{OFF}, at $V_{in} = 48\,\text{V}$, $R_L = 20\,\Omega$ and $t_{dead} = 100\,\text{ns}$.

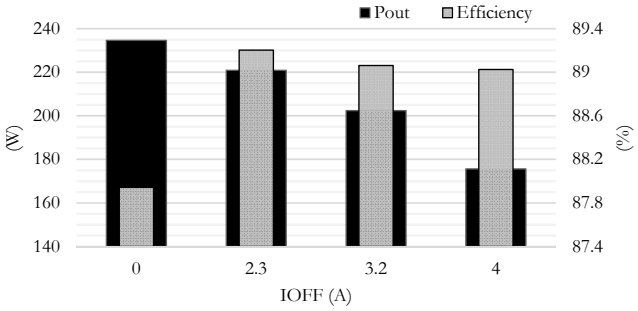

Fig. 15: Measured output power and efficiency with different I_{OFF}, at $V_{in} = 48\,\text{V}$, $R_L = 20\,\Omega$ and $t_{dead} = 200\,\text{ns}$.

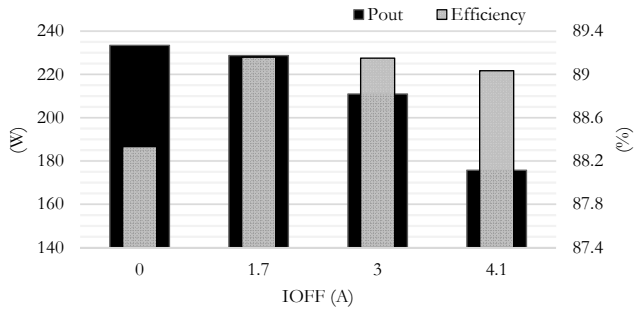

Fig. 16: Measured output power and efficiency with different I_{OFF}, at $V_{in} = 48\,\text{V}$, $R_L = 20\,\Omega$ and $t_{dead} = 400\,\text{ns}$.

they affect negatively the efficiency. Moreover, according to Fig. 5, while the efficiency is considerably affected by t_{dead}, it is clear that this is not the case for P_{out}.

- From the efficiency comparison between ZVS and ZCS operation in Fig. 7, it can be seen that the ZVS operation gives overall higher efficiency than the ZVC one. The gain in efficiency is considerable (up to 2%) especially for shorter values of t_{dead} and lower values of V_{in}. On the other hand, from the output power comparison between ZVS and ZCS operation in Fig. 6, it is clear that changing t_{dead} does not affect considerably its values. Moreover, for all the values of V_{in}, the output power is greater in ZVS than in ZCS. This result can be justified from the fact that the efficiency is also greater at ZVS and this makes its output power higher. However, at $V_{in} = 48\,\text{V}$ the difference in efficiency between the ZVS and ZCS is not that high to justify the considerable difference in output power. This means that also the input power is higher at ZVS than in ZVC. To get a better understanding of the operation of the circuit, both the absolute value $|\boldsymbol{I}_1|$ and the phase angle $\phi(\boldsymbol{I}_1)$ of the primary current $\boldsymbol{I}_1$ are plotted in Fig. 13 depending on the operating frequency f and at $V_{in} = 48\,\text{V}$. The phasor values of $\boldsymbol{I}_1$ has been derived from both (1) and (2). All the measurements have been executed at $R_L = 10\,\Omega$ which, according to (4), is equivalent to a load resistance of $R_{ac} = 8.1\,\Omega$ for the frequency domain analysis based on the equivalent circuit in Fig. 1 a). The analysis in the frequency domain of $\phi(\boldsymbol{I}_1)$ can be used to identify the operating frequencies at which both ZVS and ZCS occur. In case $\phi(\boldsymbol{I}_1)$ is equal to zero, the operation is at ZCS. On the other hand, when $\phi(\boldsymbol{I}_1)$ is negative, $\boldsymbol{I}_1$ lags V_{AB} and ZVS can be achieved. After detecting those frequencies, it is also possible to evaluate the respective values of $|\boldsymbol{I}_1|$ at ZCS and ZVS. According to Fig. 13, it is clear that $|\boldsymbol{I}_1|$ is higher at ZVS than at ZCS with the chosen resistive load $R_L = 10\,\Omega$. Consequently, the input power would also be higher. From Fig. 13 b), $\phi(\boldsymbol{I}_1)$ is zero for a large range of frequencies which is approximately 98-108 kHz. This means that the ZCS can

be achieved in several operating points and each of them gives different values of $|\boldsymbol{I}_1|$. This relatively wide range of frequencies that give zero $\phi(\boldsymbol{I}_1)$ can also be noticed in the ZCS waveforms of Fig. 11 a) and 12 a). As a result, the analyzed load case $R_L = 10\,\Omega$ is the boundary of the bifurcation-free operation, because $\phi(\boldsymbol{I}_1)$ crosses the zero only once at the nominal resonant frequency for greater values of R_L. The bifurcation phenomenon occurs when multiple resonant frequencies exist that make $\phi(\boldsymbol{I}_1)$ equal to zero. It was initially noticed by [17], [18] and more literature on that can be found in [6], [19]–[22]. In case the resistive load is doubled ($R_L = 20\,\Omega \rightarrow R_{ac} = 16.2\,\Omega$), the frequency response of $\boldsymbol{I}_1$ is considerably different than in the previous case as it is shown in Fig. 13. With $R_L = 20\,\Omega$, $|\boldsymbol{I}_1|$ is lower at ZVS than in ZCS operation. Therefore, the input power would also be lower at ZVS.

- From the analysis of the ZVS operation at higher values of I_{OFF}, it is clear that the performance is different at the two different values of R_L. According to Fig. 8, 9 and 10, at $R_L = 10\,\Omega$ there is a considerable increase in both output power and efficiency when changing the operation from ZCS to ZVS. For higher values of I_{OFF}, the reached efficiency drops again, but the output power does not drop as much as it is in the ZCS operation. Similar measurements have been done also at $V_{in} = 48\,\text{V}$, $R_L = 10\,\Omega$ and t_{dead} =100, 200, 400 ns, and their output power and efficiency are plotted respectively in Fig. 14, 15 and 16. Also in this case, there is a considerable increase in efficiency when moving the operation from ZCS to ZVS. On the other hand, the output power drops because of drop in input power as a results of the decrease of $|\boldsymbol{I}_1|$ shown in Fig. 13 a). For higher values of I_{OFF}, the output power drops dramatically while the efficiency is only slightly affected.
- The maximum efficiency measured is 89.2% at $V_{in} = 48\,\text{V}$ and $R_L = 20\,\Omega$ which is about 0.6% higher than the maximum one measured at $R_L = 10\,\Omega$.

VII. Conclusions

In this paper, the advantage of ZVS over ZCS is evaluated in terms of efficiency and delivered output power. The ZVS operation has been tuned at different input voltages and dead time conditions. The best way to tune the ZVS is through an experimental evaluation and using the theoretical model just as a support to gain an initial insight into the WPT charging system operation. Depending on the MOSFET capacitance C_{ds}, the dead time must be sufficiently large such that ZVS can be completely achieved. According to all the measurements, the best operating point of ZVS is the one with the minimum turn-off current I_{OFF} that ensures ZVS. This operating point guarantees maximum efficiency and enough delivered output power, even if the output power might be lower than in ZCS at some loading conditions. An under-estimation of I_{OFF} causes the loss of soft-switching. On the other hand, an over-estimation of I_{OFF} causes either an increase in the turn-off losses which affects the overall efficiency or a considerable drop in the delivered output power.

References

[1] K. Wu, D. Choudhury, and H. Matsumoto, "Wireless power transmission, technology, and applications [scanning the issue]," *Proceedings of the IEEE*, vol. 101, pp. 1271 – 1275, 2013.

[2] X. Lu, P. Wang, D. Niyato, D. I. Kim, and Z. Han, "Wireless charging technologies: Fundamentals, standards, and network applications," *IEEE Communications Surveys & Tutorials*, vol. 18, pp. 1413 – 1452, 2016.

[3] L. Sun, D. Ma, and H. Tang, "A review of recent trends in wireless power transfer technology and its applications in electric vehicle wireless charging," *Renewable and Sustainable Energy Reviews*, vol. 91, pp.

[4] Y. Shi, Y. Zhang, M. Shen, Y. Fan, CanWang, and M. Wang, "Design of a novel receiving structure for wireless power transfer with the enhancement of magnetic coupling," *AEU - International Journal of Electronics and Communications*, vol. 95, pp. 236–241, 2018.

[5] C.-S. Wang, G. A.'Covic, and O. H. Scelau, "General stability criterions for zero phase angle controlled loosely coupled inductive power transfer systems," in *IECON'O1: The 27th Annual Conference of the IEEE Industrial Electronics Society*, 2001.

[6] S. Chopra and P. Bauer, "Analysis and design considerations for a contactless power transfer system," *Telecommunications Energy Conference (INTELEC), 2011 IEEE 33rd International*, 2011.

[7] S. Li, W. Li, J. Deng, T. D. Nguyen, and C. C. Mi, "A double-sided lcc compensation network and its tuning method for wireless power transfer," *IEEE Transactions on Vehicular Technology*, vol. 64, 2015.

[8] S.-Y. Cho, I.-O. Lee, S. Moon, G.-W. Moon, B.-C. Kim, and K. Y. Kim, "Series-series compensated wireless power transfer at two different resonant frequencies," in *2013 IEEE ECCE Asia Downunder*, 2013.

[9] S. Li and C. C. Mi, "Wireless power transfer for electric vehicle applications," *IEEE Journal of Emerging and Selected Topics in Power Electronics*, vol. 3, pp. 4–17, 2015.

[10] R. L. Steigerwald, "A comparison of half-bridge resonant converter topologies," *IEEE Transactions on Power Electronics*, vol. 3, pp. 174–182, 1988.

[11] R. W. Erickson and D. Maksimovic, *Fundamentals of Power Electronics*, 2nd ed. Kluwer Academic Publishers, 2004.

[12] A. J. Moradewicz and M. P. Kazmierkowski, "Contactless energy transfer system with fpga-controlled resonant converter," *IEEE Transactions on Industrial Electronics*, vol. 57, pp. 3181–3190, 2010.

[13] J. D. V. W. Henry W. Koertzen and J. A. Ferreira, "Comparison of swept frequency and phase shift control for forced commutated series resonant induction heating converters," in *Conference Record of the 1995 IEEE Industry Applications Conference Thirtieth IAS Annual Meeting*, 1995.

[14] T. Kan, T.-D. Nguyen, J. C. White, R. K. Malhan, and C. C. Mi, "A new integration method for an electric vehicle wireless charging system using lcc compensation topology: Analysis and design," *IEEE Transactions on Power Electronics*, vol. 32, no. 2, pp. 1638–1650, Febraury 2017.

[15] B. Lu, W. Liu, Y. Liang, F. Lee, and J. van Wyk, "Optimal design methodology for llc resonant converter," in *IEEE Applied Power Electronics Conference and Exposition*, 2006, pp. 533–538.

[16] Infineon, *IPP030N10N5 MOSFET*, October 2016. [Online]. Available: https://www.infineon.com/dgdl/Infineon-IPP030N10N5-DS-v02_03-EN.pdf?fileId=5546d4624a75e5f1014ac4e0b47c1f49

[17] R. Laouamer, M. Brunello, J. Ferrieux, O. Normand, and N. Buchheit, "A multi-resonant converter for non-contact charging with electromagnetic coupling," in *IECON'97 23rd International Conference on Industrial Electronics, Control, and Instrumentation*, 1997.

[18] J. Boys, G. Covic, and A. Green, "Stability and control of inductively coupled power transfer systems," in *IEE Proceedings - Electric Power Applications*, 2000, pp. 37 – 43.

[19] O. Stielau and G. Covic, "Design of loosely coupled inductive power transfer systems," in *International Conference on Power System Technology*, 2000.

[20] C.-S. Wang, G. A. Covic, , and O. H. Stielau, "Power transfer capability and bifurcation phenomena of loosely coupled inductive power transfer systems," *IEEE Transactions On Industrial Electronics*, vol. 51, no. 1, pp. 148–157, Feb. 2004.

[21] C.-S. Wang, O. Stielau, and G. Covic, "Design considerations for a contactless electric vehicle battery charger," *IEEE Transactions on Industrial Electronics*, vol. 52, pp. 1308 – 1314, 2005.

[22] M. Iordache, L. Mandache, D. Niculae, and L. Iordache, "On exact circuit analysis of frequency splitting and bifurcation phenomena in wireless power transfer systems," in *International Symposium on Signals, Circuits and Systems (ISSCS)*, 2015.